

Combined optical tweezers and laser dissector for controlled ablation of functional connections in neural networks

Francesco Difato, Marco Dal Maschio, Emanuele Marconi, Giuseppe Ronzitti, Alessandro Maccione, Tommaso Fellin, Luca Berdondini, Evelina Chierigatti, Fabio Benfenati, and Axel Blau

Italian Institute of Technology, Department of Neuroscience and Brain Technologies, Via Morego 30, Genoa, 16163 Italy

Abstract. Regeneration of functional connectivity within a neural network after different degrees of lesion is of utmost clinical importance. To test pharmacological approaches aimed at recovering from a total or partial damage of neuronal connections within a circuit, it is necessary to develop a precise method for controlled ablation of neuronal processes. We combined a UV laser microdissector to ablate neural processes *in vitro* at single neuron and neural network level with infrared holographic optical tweezers to carry out force spectroscopy measurements. Simultaneous force spectroscopy, down to the sub-pico-Newton range, was performed during laser dissection to quantify the tension release in a partially ablated neurite. Therefore, we could control and measure the damage inflicted to an individual neuronal process. To characterize the effect of the inflicted injury on network level, changes in activity of neural subpopulations were monitored with subcellular resolution and overall network activity with high temporal resolution by concurrent calcium imaging and microelectrode array recording. Neuronal connections have been sequentially ablated and the correlated changes in network activity traced and mapped. With this unique combination of electrophysiological and optical tools, neural activity can be studied and quantified in response to controlled injury at the subcellular, cellular, and network level. © 2011 Society of Photo-Optical Instrumentation Engineers (SPIE). [DOI: 10.1117/1.3560268]

Keywords: holography; optical tweezers; laser dissection; neural network; microelectrode array electrophysiology; force spectroscopy.

Paper 10342RR received Jun. 18, 2010; revised manuscript received Feb. 1, 2011; accepted for publication Feb. 7, 2011; published online May 2, 2011.

1 Introduction

Neuronal networks *in vitro* represent an intermediate model situated between single neurons and brain tissue for studying neural development, coding, pharmacology, pathology, and regeneration. Understanding network dynamics requires techniques capable of monitoring the activity of an elevated number of neurons at high temporal resolution. Over the last decade, two core approaches have been favored. One of them is based on optics, as a low invasive tool for imaging the activity of many cells with subcellular resolution over a field of view of a few hundred micrometers.¹ The other is the electrical extracellular recording of network activity by means of microelectrode array (MEA) devices,² which allow the multisite monitoring of several neurons with submillisecond resolution around a limited number of electrodes distributed over a few square millimeters. Several laboratories started to combine these two methods to compensate for their complementary shortcomings in resolving and extracting neural network properties.³

The properties of the culture substrate represent an important aspect of *in vitro* systems. The viscoelastic behavior of a neurite is assumed to result from the interaction of cytoskeletal components with the extracellular matrix (ECM).⁴ Indeed, not only chemical but also mechanical properties of the ECM

can regulate cellular properties such as shape, polarity, motility, and morphological phenotypes. Alteration in the interactions between a cell and its surrounding ECM may result in apoptosis, malignant transformation, or loss of tissue architecture.⁵ The ability of a laser dissection system to selectively ablate subcellular compartments without damaging adjacent structures offers new possibilities for studying cell-ECM interactions^{6,7} or axonal regeneration.^{8,9}

In this work, we present the design and evaluate the performance of a system that combines two optical manipulation techniques, holographic optical tweezers (OTs), and a laser microdissector (LMD), to directly quantify the mechanical perturbation produced by laser ablation in a neurite, and to study *in vitro* regeneration of cellular processes after well-calibrated, laser-inflicted damage. Moreover, the system is configured to work in combination with fluorescence imaging and MEA electrophysiology to track and dissect neuronal interconnections for elucidating their local and network-wide role. For this purpose, we used low-density neural cultures to evaluate the architecture of the neural network, and to achieve higher spatial control of the neuronal connections we dissect and the structural changes we impose on the network itself.

The presented system will be applied to the study of processes involved in the early stages of neuronal differentiation,

Address all correspondence to: Francesco Difato, Italian Institute of Technology, Department of Neuroscience and Brain Technologies, Via Morego 30, 16163 Genoa, 16163 Italy, Tel: 0039 010 71781739; Fax: 0039 010 7170321; E-mail: Francesco.difato@iit.it.

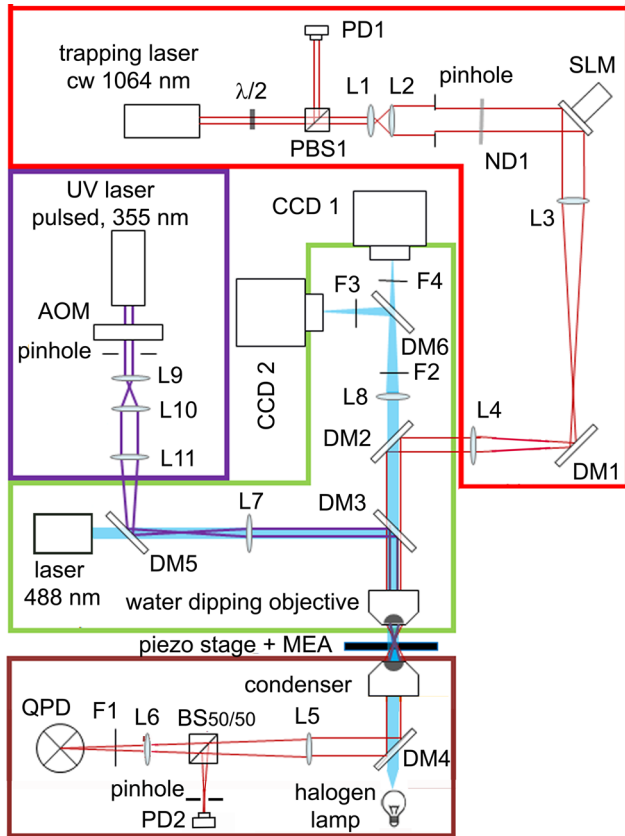


Fig. 1 Schematic optical layout of the instrument. Color box legend: Upright optical tweezers (red), a laser microdissector (violet), and a back-focal plane interferometer (brown) are operated on an Olympus BX51 microscope (green). AOM: acousto-optic modulator; BS_{50/50}: beam splitter 50/50%; CCD: charged coupled device camera; DM: dichroic mirror; F: filter; $\lambda/2$: half-wave plate; L: lens; MEA: microelectrode array amplifier; ND: neutral density filter; PBS: polarizing beam splitter; PD: photodiode; QPD: quadrant photodiode.

with particular focus on neurite regeneration and neural network dynamics.

2 Material and Methods

2.1 Optical Tweezers Setup

As depicted in Fig. 1, the OT setup (red and brown box) is based on an ytterbium continuous wave fiber laser operating at 1064 nm (IPG Laser GmbH). The laser beam is expanded with a telescope, composed of a 35 mm and 100 mm focal length doublet (L1 and L2, IR doublets – Thorlabs), and projected onto a spatial light modulator (SLM) (LCOS-SLM, model X10468–07, Hamamatsu: 800×600 pixel resolution, pixel dimension: $20 \times 20 \mu\text{m}^2$, phase modulation: 0 to 4π , wavelength range: 680 to 1100 nm, 60 Hz refresh rate), before entering into a modified upright microscope (BX51, Olympus; green box). The computer-generated diffraction pattern at the SLM modulates the laser beam wavefront.

The SLM plane and the back focal plane of the microscope objectives are optically conjugated by a second telescope, made of two lenses in 4-f configuration both with focal lengths of 200 mm, to cover the distance between the SLM plane and the

pupil plane (L3 and L4; IR doublets, Thorlabs). The structured laser light enters the microscope through an auxiliary port (adapted U-DP Olympus microscope component), which was originally designed for the lateral attachment of a CCD camera. The beam is reflected perpendicularly onto the optical axis of the microscope by a low pass dichroic mirror (DM2; 765dcspxr, Chroma). It then passes through a second dichroic mirror used for fluorescence imaging (DM3 selectable dichroic mirror: FF510-DI01, FF593-Di02, FF395/495/610-Di01, Semrock) before reaching the objective. DM3 is part of a standard filter cube situated in the filter cube wheel of the microscope. Emission filters have been relocated to external multiposition filter carriers (F3 and F4) in front of the two CCD cameras (CCD1 and CCD2), and excitation filters have been removed. In combination with the microscope tube lens (L10) and with an additional low pass emission filter (F2; ET750SP-2p8, Chroma) above DM2, this layout ensures that only the visible portion of the light returning from the sample can reach the CCD cameras. Stray, residual, or back-reflected infrared (IR) laser light is rejected. A dichroic mirror (DM7) in front of CCD1 and CCD2 separates and distributes the light coming from the sample onto the two CCD cameras (CCD1: iXon V887ECSUVB EMCCD, Andor: 512×512 pixels, back illuminated sensor; CCD2: BASLER-Pilot, 04-PIA1000-48GM CCD, 1004×1004 pixels, 48 Hz full frame rate). Thus, with an appropriate choice of DM7, F3, and F4 (FF562-DI02, FF01-520/35, Semrock), bright field and fluorescence calcium imaging can be performed simultaneously.

A laser diode (TECBL-30G-488, World Star Tech. Inc.) that can be modulated by TTL pulses is the light source for fluorescence calcium imaging. A halogen lamp serves as the bright field illumination source (KL2500LCD COLD LIGHT 230VKL, Olympus). The latter is equipped with a filter wheel to select a color range which does not interfere with the emission spectra of the fluorochromes used to label the sample (BLP01-561R, Semrock).

Infrared light interference fringes in the back focal plane of the objective condenser are directed by the low pass dichroic broadband mirror DM4 onto a four-quadrant photodiode (QPD, S5980 with C5460SPL 6041 board, Hamamatsu) and a photodiode PD2 (PDA100A-EC, Thorlabs) for force-spectroscopy measurements, while visible light from the halogen lamp can pass through. The objective condenser, together with DM4, L5, L6, BS50/50 (700 to 1100 nm broadband nonpolarizing beam splitter cube, BS014, Thorlabs), F1 (LL01-1064-12.5, Semrock), and PD2 are mounted onto a metal framework (brown box). It can be aligned manually with respect to the microscope stage and to the QPD by three manual translation stages (PT3/M, Thorlabs). The QPD is mounted on a separate x, y, z stage and quantifies the lateral displacement of a probe in the optical trap. PD2 with a pinhole mask in front of it provides a signal proportional to the axial position of the trapped probe. Electrical signals coming from the four quadrants of the QPD and PD2 are amplified 100-fold (2 amplifier boards: MULTIBOARD, Sglux) and then digitized independently by an analog-to-digital (A/D) data acquisition converter (PCI-4462, 24 bit, 4 channels, 204.8 k Samples/second, National Instruments).

The stage of the microscope is composed of a 3-axis linear dc motor micro-positioning system (M-126.CG1, Physics-Instruments) carrying a separate 3-axis piezoelectric nanopositioning stage (P-733.3DD, Physics-Instruments) to combine

coarse movement of the sample with the sub-nanometer resolution of the piezo stage.

2.2 Laser Microdissector Setup

A pulsed sub-nanosecond UV Nd:yttrium–aluminum–garnet laser at 355 nm (PNV-001525-040, PowerChip nano-Pulse UV laser, Teem Photonics), is the light source of the LMD setup (violet box). The first diffraction order intensity of the laser beam is controlled by an acousto-optical modulator (AOM) (MQ110-A3-UV, 355 nm fused silica, AA-Opto-electronic); the nondiffracted zero order is filtered out by a pinhole. The laser beam passes an expander (L9 and L10: 35 and 150 mm UV plano-convex UV fused silica lenses, respectively, Lambda) and a 75-mm lens (L11 plano-convex UV fused silica lens, Lambda) before entering the microscope (green box). To couple the laser dissector path with the microscope, all optics had to be removed from the epi-illuminator and be replaced by a 125-mm UV lens just before the filter cube wheel (L7 plano-convex UV fused silica lens, Lambda). This lens forms a telescope with L11 and is conjugated with the back focal plane of the objective.

The diaphragm of the epi-illuminator was substituted by a narrow-band laser mirror, which reflects 355-nm laser light while letting light pass from the 488-nm laser diode (DM6, TLM1-350-45-P, CVI) used for fluorescence microscopy. As mentioned in Sec. 2.1, the excitation filters were removed from the filter cubes. Thus, fluorescence imaging and laser dissection can be performed simultaneously.

2.3 System Control and User Interface

A custom-made software interface based on LabVIEW (National Instruments) controlled the IR laser intensity, the UV laser intensity, and its pulse repetition rate. It acquired the images from the BASLER CCD camera and samples from the QPD and PD2. Images from the Andor CCD camera were acquired by a separate software package (SOLIS) provided by the manufacturer. Holograms for the spatial light modulator were generated by the freely available Blue-tweezers software (Optics Group, Physics and Astronomy, University of Glasgow, <http://www.physics.gla.ac.uk/Optics/projects/tweezers/slmcontrol/>). Synchronization signals between devices were sent through a D/A board (PCI-6529, 24 bit, 4 channels, 204.8 kSamples/second, National Instruments). Two independent analog input channels of the MEA setup acquired the trigger of the blue laser diode and the Andor CCD used for calcium imaging, and the trigger of the UV laser pulses.

2.4 MEA Electrophysiology

Multisite neural network activity was recorded extracellularly by using a commercially available MEA recording setup (Multi Channel Systems, Germany). It featured a 60-channel amplifier for upright microscopy with a built-in thermal sensor and heating element, an external temperature controller, a 64-channel PCI-bus A/D conversion card, and a software interface. Standard MEAs (500/30iR-Ti) with a 6×10 electrode matrix layout were used.

2.5 Bead Coating

Silica beads (\varnothing 4 μm , COOH coated, Bangs Laboratories) had been coated with fibronectin following the procedure described in the PolyLink Protein Coupling Kit (Polysciences).

2.6 Preparation of MEA Substrates

MEAs (500/30iR-Ti, Multi Channel Systems) were immersed in ultrapure water (MilliQ) for one day. The day before cell seeding, substrates were hydrophilized by oxygen plasma treatment (30 Pa, 60 W, 2 min) and coated with 150 μl poly-D-lysine (100 $\mu\text{g}/\text{ml}$, Sigma) to support cell adhesion. MEAs were sterilized under UV, incubated overnight in a standard humidified CO_2 cell culture incubator (5% CO_2 , 92% relative humidity, 37°C), washed once with sterile ultrapure water, and filled with cell culture medium, which was removed just before cell seeding.

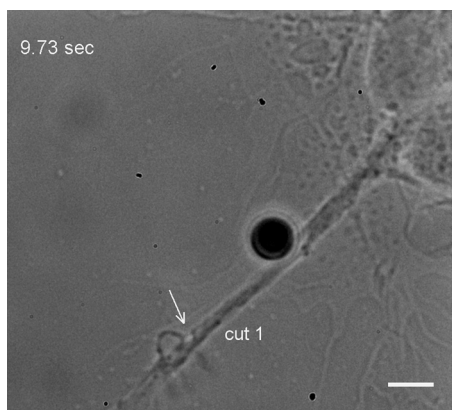
2.7 Cell Cultures

Primary cultures were obtained from the brain tissue of Sprague Dawley rats at embryonic day 18 (E18) following published procedures.¹⁰ In summary, embryos were removed and dissected under sterile conditions. Hippocampi were dissociated by enzymatic digestion in trypsin (0.125% for 20 min at 37°C). Trypsin activity was blocked by adding complete media (Neurobasal (Gibco) supplemented by B27 (2%, Gibco), alanyl-glutamine (2 mM, Gibco), penicillin/streptomycin (both 1 mM, Sigma) containing 10% fetal bovine serum (FBS, Gibco). After trypsinization, tissues were rinsed in complete media without FBS, and triturated with a fire-polished Pasteur pipette. Neurons were plated at a concentration of 0.25 to $1 \cdot 10^5$ cells/ml on glass-bottom plastic Petri dishes (P35G-0-14-C, MaTek Corporation) and in small volumes (10 to 40 μl) at nominal density of 70 cells/ mm^2 onto MEAs. They were left in the incubator for less than 2 h to allow for cell attachment to the culture substrate before filling the cell culture containers up to 2/3 of their volume with serum-free medium of the above-mentioned composition. Forty percent of the medium volume was exchanged every week. Spontaneous electrical activity could be recorded after 10 days *in vitro* (DIV).

For quantifying LMD-inflicted damage at an early age, hippocampal neurons at 3 to 7 DIV seeded on glass-bottom Petri dishes were incubated for 10' with 5 μm Fluo-4 AM (Invitrogen). Hippocampal neurons on MEAs at 10–18 DIV were incubated for 20' with 5 μm Fluo-4 AM.

2.8 Microscope Sample Chamber

Cells under the microscope were kept at 35°C by a Peltier device (QE1 resistive heating with TC-344B dual channel heater controller, Warner Instruments). Using a custom-made gravity-propelled perfusion inlet and a vacuum aspiration outlet, dye-loaded cells were rinsed and perfused at ≤ 0.3 ml/min with artificial cerebrospinal fluid consisting of (in mM): 135 NaCl, 5 KCl, 0.4 KH_2PO_4 , 0.75 MgSO_4 , 1.5 CaCl_2 , 20 HEPES (pH 7.4), and 5.6 glucose.



Video 1 Bright field time lapse imaging during neurite laser dissection. Time lapse bright field imaging of rat hippocampal neuron (7 DIV) to monitor the thinning of the neurite upon dissection until its complete disruption. Numbers indicate seconds. Bar is 10 μ m. Frame rate is 7 Hz (see Fig. 2). (QuickTime, 3.7 MB) [URL: <http://dx.doi.org/10.1117/1.3560268.1>]

3 Results

During differentiation, neurons change their shape to explore the extracellular environment and extrude processes to establish connections with other cells. Once the connections are formed, the components of the cytoskeleton rearrange to produce tension on the connection site and stabilize the architecture of the network.¹¹ Here, we demonstrated how the release of tension in a neural connection could be directly quantified through back focal plane interferometric (BFPI) tracking of a membrane-bound bead kept in an optical trap,^{12,13} while a laser dissector was progressively damaging a neurite and perturbing the mechanical equilibrium of its cytoskeleton. Rat hippocampal neurons (7 DIV) were loaded *in vitro* with the calcium indicator Fluo-4 AM to monitor calcium entry upon dissection of their processes. During laser ablation of a neurite, simultaneous time-lapse bright field, and fluorescence imaging documented the thinning of the neurite until its complete disruption [(Fig. 2(a)) and the resulting calcium influx into the cell (see supplementary Videos 1 and 2) as quantified by $(F-F_0)/F_0$ in the region of interest [(Fig. 2(b), red ROI in the last frame)].

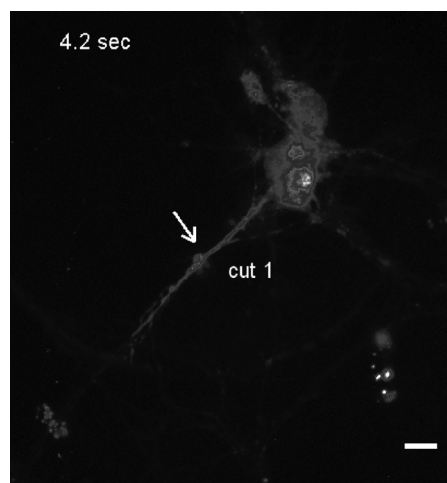
Fibronectin-coated beads were optically trapped and moved into close proximity of the neurite to be dissected.¹⁴ The position of the trapped probe with respect to the neurite and to the focal spot of the UV laser dissection, was controlled by displaying a dynamically generated hologram on the SLM. The trapped probe was positioned 2 μ m above the coverslip and about 20 μ m away from the UV laser spot. The trap stiffness, $K_{x,y,z}$ (k_x, k_y, k_z), and the detector sensitivity were calibrated using the power spectrum method, when the bead had no contact with any structure.¹⁵ The UV laser pulses had no influence on the power spectrum of the trapped bead.¹⁶ Adhesion events between the fibronectin-coated bead and the integrins in the plasma membrane of a neurite were monitored by changes in the variance of the Brownian motion of the bead. When the bead was far from the neurite, the total variance ($\sigma_t^2 = \sigma_x^2 + \sigma_y^2 + \sigma_z^2$) was 568 nm²; it decreased to 265 nm² when the bead adhered to the membrane.¹⁷

BFPI therefore allowed the simultaneous quantification of the released tension in the damaged neurite with nanometer and

submillisecond resolution [Fig. 2(d)]. Upon complete retraction of the neurite, the bead remained in the laser trap. The total variance in its Brownian motion came back to the value measured before it adhered to the cell membrane. This approach neither required any assumptions on the organization of the cytoskeleton components in the neurite nor its modeling as a homogeneous viscoelastic solid. Figure 2(c) depicts the cumulative energy release by the UV laser during the experiment. The damage to the neurite could be controlled from partial to complete ablation by varying either the number of delivered pulses or the energy per pulse.

During the first 25 s, 2000 pulses with energy of 20 nJ per pulse were delivered. Local calcium influx at the stimulated site and its subsequent spread toward the soma was visible shortly after the first pulses had been delivered at 3.6 s [Fig. 2(b)]. Administering a high number of low-energy pulses led to partial damage only, even at 70 s [Fig. 2(a)]. For the period of subsequent five exposures to UV light pulses [Fig. 2(c)], we monitored the force on the adhered probe. However, if the energy per pulse was increased while the number of pulses was decreased, a complete ablation of the process required only 200 pulses at energies of 65 nJ per pulse [Figs. 2(a) and 2(c) after 70 s]. Once the UV laser damage inflicted to a neuron was calibrated and quantified, UV surgery could be performed with high spatio-temporal control. Figures 3, 4 and 5 show the importance of this approach for neural regeneration and functional network interconnectivity studies.

Two types of localized surgery on a neural network are shown in Fig. 3. In Fig. 3(a), 150 pulses at energy of 67 nJ per pulse were sufficient to completely cut a neurite at a distance of about 30 μ m from the soma. In consequence of the cut, the distal part of the neurite degenerated while the proximal part of the neurite formed an exploring growth cone after 7 min. The last two frames show how the growth cone changes orientation to explore its surroundings, and to recreate the connection to the network (see Video 3).



Video 2 Fluorescence calcium time lapse imaging during neurite laser dissection. Time lapse fluorescence imaging of rat hippocampal neuron (7 DIV) loaded with the calcium indicator Fluo-4 AM to monitor calcium entry upon dissection of its process. Numbers indicate seconds. Bar is 12 μ m. Frame rate is 5 Hz (see Fig. 2). (QuickTime, 3.7 MB) [URL: <http://dx.doi.org/10.1117/1.3560268.2>]

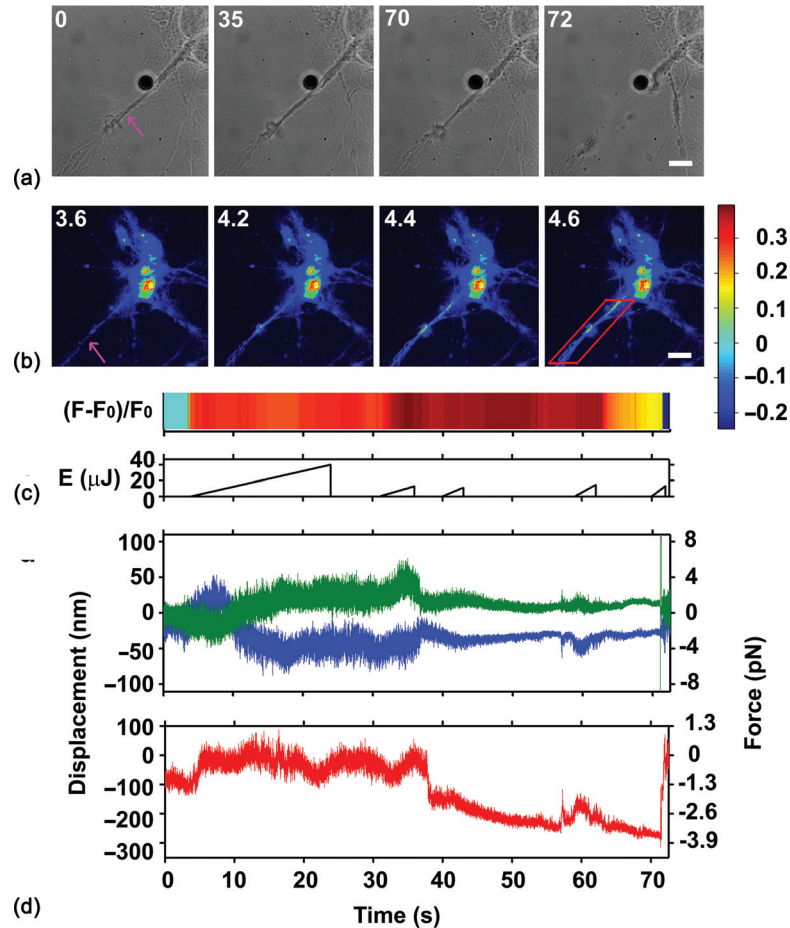


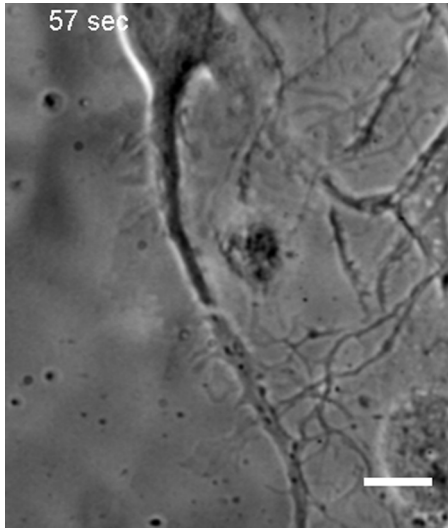
Fig. 2 Laser dissection of a single neurite and measurements of the released tension. (a) Bright field images of a differentiating rat hippocampal neuron (7 DIV). The violet arrow indicates the dissection site on the neurite (Video 1). Frame rate was 7 Hz. The numbers indicate seconds. Bar: 10 μm . The pulse repetition of the UV laser was 100 Hz. A bead ($\text{O} 4 \mu\text{m}$) coated with fibronectin was trapped and positioned on the neurite to adhere to integrins in the plasma membrane. The power of the IR laser at the sample was 40 mW. Objective: 60 \times , NA 0.9 (Olympus). The trapping stiffness was calibrated by the power spectra method: $k_{x,y} = 80 \text{ pN}/\mu\text{m}$, $k_z = 13 \text{ pN}/\mu\text{m}$. (b) Fluor-4 AM fluorescence of the neuron in (a). Average power at the sample of the 488 nm laser diode was 50 μW . Repetition rate of the laser diode was 5 Hz with a duty cycle of 4%. Frame acquisition rate was 5 Hz. Numbers indicate seconds. Bar: 12 μm (Video 2). The red ROI in the last frame indicates the region for quantifying the $(F-F_0)/F_0$ fluctuations in color-coded fluorescence intensity (F_0 was the intensity value in the first frame of the video). (c) Time course of the energy delivered by the UV laser to the sample. (d) Displacement of and force on the trapped bead versus time. Green and blue traces are the x , y components; the red trace is the z component. Sampling rate was 10 kHz.

Figure 3(b) shows the partial dissection of a neurite of a differentiating rat hippocampal neuron at 4 DIV upon delivery of 190 pulses at energy of 30 nJ per pulse. In this case, only a thinning of the process was observed at the dissection site without loss of the connection with the distal part of the neurite. With the cut performed at low energy per pulse, the distal part of the neurite did not degenerate, and the complex motility of the growth cone was preserved during the dissection and thereafter (see Video 4). Six minutes later, healing and fast regeneration of the neurite occurred. After 20 min, the process integrity appeared completely recovered.

These experiments not only demonstrate the high degree of control over the site and type of induced damage, but also the possibility of tracking and documenting the regeneration process in real time. Moreover, these results show that UV laser ablation experiments can be performed during the first days after cell plating, usually a critical differentiation period in *in vitro* experiments. In most cases, laser dissection experiments *in vivo*

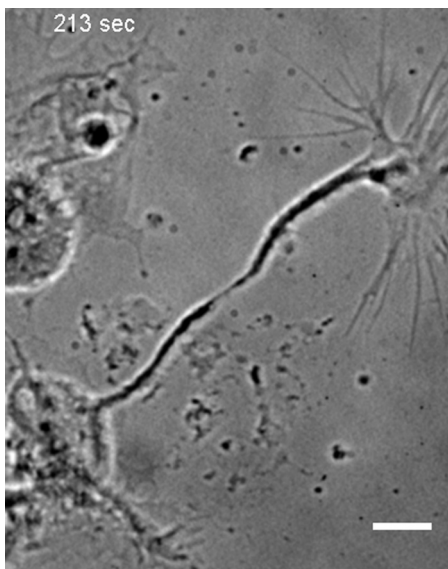
are carried out with lasers having longer wavelengths.⁹ However, for *in vitro* preparations, a pulsed UV laser has two advantages: it creates a smaller diffraction-limited spot and exposes the cell to a low average power, thus shortening the exposure time and minimizing undesirable thermal effects at the sample.^{8,18} This gives high spatial control over the surgical process, narrowing the nonlethal ablation distance to the cell body to a few tens of micrometers and avoiding irreversible damage to the cell during differentiation.

The precision of the system opens the door to functional interconnectivity studies. Spontaneous activity of a low-density network of hippocampal neurons (rat, 18 DIV) on a MEA was recorded continuously at 25 kHz while sequentially dissecting individual connections to pinpoint correlated activity changes. Simultaneous calcium imaging of a subpopulation of neurons near the dissection site revealed local activity with single cell resolution. Although neurons plated at low-densities are more difficult to maintain, and less neurons are sufficiently close to



Video 3 Complete neurite dissection and growth cone formation. Complete cut of a neurite by 150 pulses of the UV laser at energy of 67 nJ per pulse. After complete dissection of the neurite, a new growth cone is formed at the tip and starts to navigate to find the path to re-establish a connection. Numbers indicate seconds. Bar is 10 μm . Frame rate 0.3 Hz (see Fig. 3). (QuickTime, 3.1 MB) [URL: <http://dx.doi.org/10.1117/1.3560268.3>]

the electrode to yield recordable signals, single units and connections in the network can be visualized more easily. Thus, their network architecture is more accessible to modifications. Figure 4(a) shows a mosaic of two bright field images acquired around 1 (electrode 27) out of 60 electrodes of the MEA chip. Numbered lines indicate the location and succession of cutting connections. Figure 4(b) displays the same region as a mosaic



Video 4 Partial neurite dissection and regeneration. Partial damage inflicted to a neurite by 190 pulses of the UV laser at energy of 30 nJ per pulse. The video shows the thinning of the process at the dissection site, without loss of the connection with the distal part of the neurite, and its fast regeneration. Numbers indicate seconds. Bar is 10 μm . Frame rate 0.3 Hz (see Fig. 3). (QuickTime, 3.0 MB) [URL: <http://dx.doi.org/10.1117/1.3560268.4>]

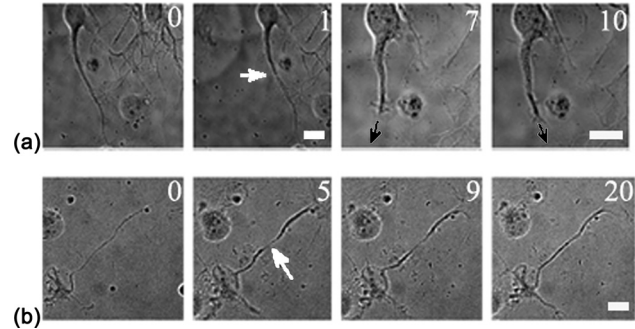


Fig. 3 Laser dissection of single neurons in neural networks. (a) Complete neurite dissection and regeneration of a hippocampal neuron (rat, 4 DIV). The white arrow indicates the dissection site. The numbers indicate minutes. The pulse repetition of the UV laser was 100 Hz, the average power at the sample about 7 μW . The black arrows in the last two frames illustrate the orientation of the exploratory motion of the regenerating growth cone after dissection. Bars: 12 μm (Video 3). (b) Partial dissection and regeneration of a hippocampal neuron (rat, 3 DIV). The white arrow indicates the dissection site. Numbers indicate minutes. The pulse repetition rate of the UV laser was 100 Hz, the average power at the sample 3 μW . As seen in the last frame, the neurite appears completely recovered after 20 min. Bar: 25 μm (Video 4).

of five fields of view acquired by fluorescence calcium imaging. Numbered circles indicate the single units and integration areas for plotting fluorescence fluctuations over time (Fig. 5). Considering that the laser dissector spot was positioned on the neurite to be ablated by motion of the stage, the number of cells from which we recorded calcium fluctuations depended on the field of view of the acquired images.

By combining electrophysiological and fluorescence recording techniques, network-wide activity could be monitored electrically by the 60 electrodes while the contribution of individual neurons to the signal recorded from a specific electrode could be estimated from calcium fluctuations (Fig. 4). Dissecting individual connections without irreversibly damaging the neuron allows identifying its contribution to the overall network activity.

Figure 5 shows the changes in the network activity during the lesion of some of its processes [as depicted in Fig. 4(b)] in eight subsequent experimental sessions (S1–S8). S1 shows basal calcium fluctuations in cell 1, which was the cell closest to electrode 27. The dissection of processes in its vicinity [white bars in Fig 4(b)] started after 480 s. Until S3, after the ablation of six different processes, cell 1 presented spontaneous activity. At the seventh cut, cell 1 showed a high calcium influx and became silent. In S5, average activity on electrode 27 decreased to 1/3. In contrast, activity on electrode 41, which was about 2.5 mm away from electrode 27, became less sparse and mainly organized in bursts. The trend is summarized in the inset graph as the total number of recorded spikes from these two electrodes in each experimental session.

In S5, the 11th cut produced a calcium wave in the neighboring cells. After a while (about 200 s), cells recovered their basal calcium levels with the exception of cell 3, which maintained an elevated calcium level until S8. This suggests that the damage inflicted to the neurite in cut 11 belonged to cell 3. Nonetheless, spontaneous activity stayed until synchronized with activity in other cells and those contributing to the spiking on electrodes 27 and 41.

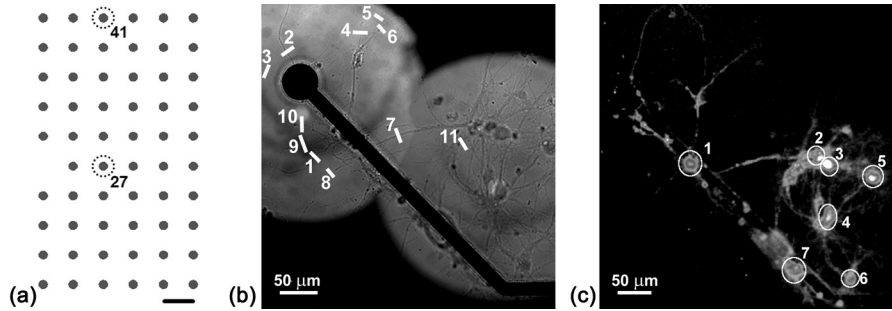


Fig. 4 Laser dissection of individual connections in a neural network on a MEA. (a) Electrode layout of the MEA chip: 6×10 matrix of electrodes with a diameter of 30 μm and an electrode spacing of 500 μm (= black bar). The strongly correlated activity on electrodes 41 and 27 was used for the analysis shown in Fig. 5. (b) Mosaic of two bright field images of the neural network around one electrode (#27) of such 60-electrodes MEA. White lines indicate the dissected connections and numbers the dissection sequence. (c) Mosaic of five fluorescence images of the network in (b) loaded with Fluo-4 AM. Circles and numbers indicate cells and approximate areas from which calcium fluctuations were quantified.

4 Discussion

The integration of optical and electrophysiological techniques is becoming an emerging method for studying neural circuits *in vitro*. In the present study, we demonstrated how precisely calibrated laser surgery on neural networks can serve as an experimental model for network computation and regeneration studies. In the first experimental configuration, we illustrated how the energy of the laser dissection system can be fine-tuned by just two parameters, the number of pulses per time and the energy per pulse. In particular, we showed how the modulation of the energy delivered to the sample differently affected the morphological, chemical, and mechanical damage inflicted to

a cell. Changes in the morphology of the process were documented by bright field imaging, while calcium imaging gave an estimate of the extracellular solution influx into the cell before the resealing of its membrane.

Furthermore, we could directly quantify the released tension in a neurite upon disruption of the cytoskeletal components by interferometric force spectroscopy without need for any theoretical cell modeling.^{6,7} Several papers reported on the importance of combining optical manipulation techniques as laser dissectors and optical tweezers.¹⁹ In this work, we present, for the first time to our knowledge, the possibility of performing laser dissection and force spectroscopy simultaneously, to calibrate

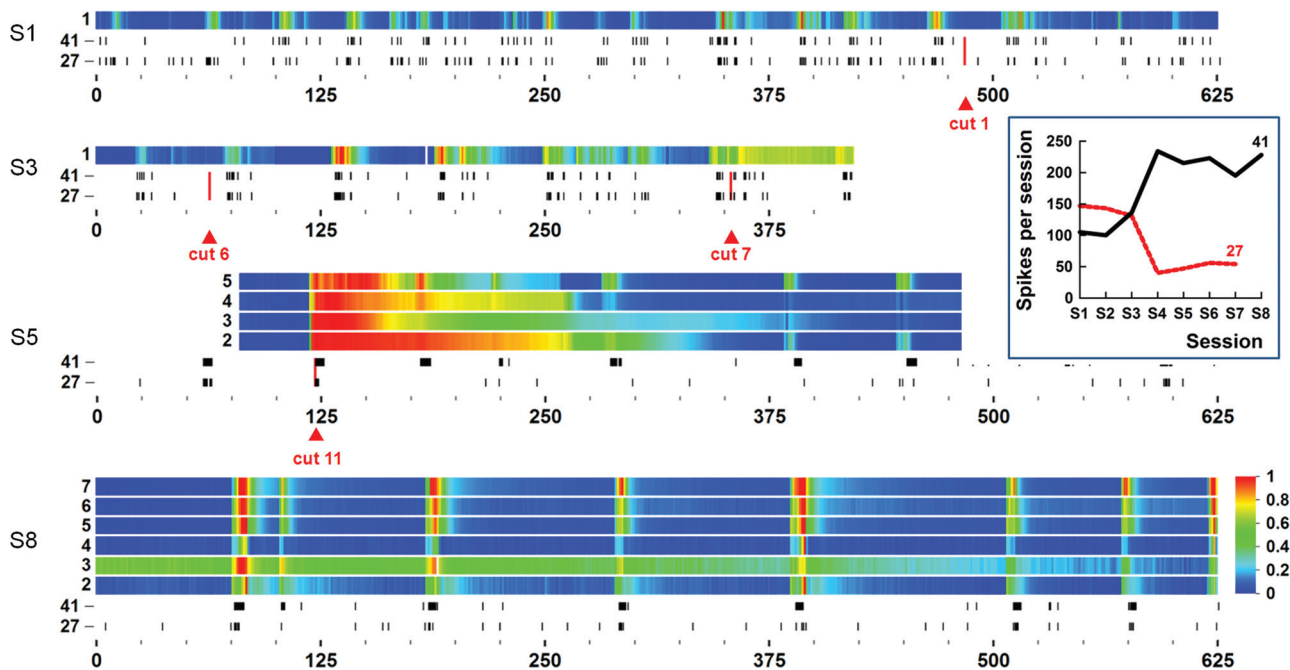


Fig. 5 Spontaneous activity of a neural network recorded simultaneously by MEA electrodes and calcium fluorescence imaging during subsequent ablation of neuronal connections. The recording of network activity was divided into eight experimental sessions (S1÷S8) each lasting 625 s; four of them are depicted. Color-coded calcium fluctuations from the seven cells shown in Fig. 4(b) were temporally aligned with extracellularly recorded electrical activity from electrodes 41 and 27. Calcium fluctuations were quantified as $(F - F_0)/F_0$, with F_0 equal to the minimum intensity measured in each video session, to obtain fluctuation values above zero. Moreover, intensities of individual cells were normalized to their maximum intensity during an experimental session to obtain the same color legend for all experimental sessions. Dissection events during the experimental sessions are marked by vertical red lines; numbers correspond to those in Fig. 4. The inset displays the change in the total number of recorded spikes from electrodes 27 and 41 during each session.

and quantify the laser ablation process with sub-pico-Newton and millisecond resolution.

An increasing number of works point out the importance of a mechanical equilibrium between the tensile force of the cytoskeleton and the elastic resistance of the extracellular matrix,^{20,21} and how the cell is exploring the mechanical properties of the substrate during differentiation.¹² The quantification of the released tension during laser surgery, besides giving an estimate of the damage inflicted to a cell,²² can be used to characterize and catalogue type age-specific tensile forces in different neurites and neurons. This knowledge will lead to a better understanding of how the intercellular organization of a network is steered toward mechanical equilibrium,^{23,24} and how neuro-degenerative pathologies affecting cytoskeleton components may alter this equilibrium. Moreover, it offers the possibility to study how changes in the extracellular matrix²⁵ of cells in culture can modify the cell-substrate interactions.

The use of a pulsed UV-A laser with very short pulse duration (400 ps) permits laser surgery at extremely low average power (few μW) at the sample, thereby confining unwanted thermal effects. We exemplarily demonstrated this by dissecting neural processes close to their cell bodies during the first days of differentiation. In future studies, this feature may be exploited to better characterize neural polarization and regeneration after neurite ablation.²²

In the last experimental configuration, we presented the simultaneous local calcium imaging and electrophysiological MEA recording of network-wide activity.³ We reported on its implementation with a low invasive laser dissection system for getting new insights into network architectures and the functional contributions of individual neurons or their sub-cellular compartments.

Future improvements of the system are underway, such as the development of a multipoint force spectroscopy system which combines the holographic optical tweezers with fast optical imaging.²⁶ This will allow the tracing and quantification of the tension release and its propagation in space and time in order to characterize the mechanical organization of the network, quantify its damage, and study the effect on its activity. Furthermore, the holographic optical tweezers will be used for local cell stimulation with functionalized beads²⁷ to study and stimulate the regeneration process.

Acknowledgments

We thank Dan Cojoc for help in setting up the optical tweezers, Julien Colombelli for valuable discussions in developing the laser dissector system, and Giacomo Pruzzo and Alessandro Parodi for the development of custom electronics and software. Special thanks are expressed to Francesca Succol and Marina Nanni for their expert advice and assistance in cell culture preparation. This work was supported by grants from Telethon-Italy (GGP10109 to E.C., GGP09134 to F.B. and GGP10138 to TF), and from Compagnia di San Paolo to T.F.

References

1. M. Dal Maschio, F. Difato, R. Beltramo, A. Blau, F. Benfenati, and T. Fellin, "Simultaneous two-photon imaging and photo-stimulation

- with structured light illumination," *Opt. Express* **18**(18), 18720–18731 (2010).
2. L. Berdondini, K. Imfeld, A. Maccione, M. Tedesco, S. Neukom, M. Koudelka-Hep, and S. Martinoia, "Active pixel sensor array for high spatio-temporal resolution electrophysiological recordings from single cell to large scale neuronal networks," *Lab Chip* **9**(18), 2644–2651 (2009).
3. W. L. Shew, T. Bellay, and D. Plenz, "Simultaneous multi-electrode array recording and two-photon calcium imaging of neural activity," *J. Neurosci. Methods* **192**(1), 75–82 (2010).
4. D. E. Ingber, "Tensegrity II. How structural networks influence cellular information processing networks," *J. Cell Sci.* **116**(Pt 8), 1397–1408 (2003).
5. S. R. Peyton, C. M. Ghajar, C. B. Khatiwala, and A. J. Putnam, "The emergence of ECM mechanics and cytoskeletal tension as important regulators of cell function," *Cell Biochem. Biophys.* **47**(2), 300–320 (2007).
6. J. Colombelli, A. Besser, H. Kress, E. G. Reynaud, P. Girard, E. Caussinus, U. Haselmann, J. V. Small, U. S. Schwarz, and E. H. Stelzer, "Mechanosensing in actin stress fibers revealed by a close correlation between force and protein localization," *J. Cell Sci.* **122**(Pt 10), 1665–1679 (2009).
7. K. Tanner, A. Boudreau, M. J. Bissell, and S. Kumar, "Dissecting regional variations in stress fiber mechanics in living cells with laser nanosurgery," *Biophys. J.* **99**(9), 2775–2783 (2010).
8. Y. T. Kim, K. Karthikeyan, S. Chirvi, and D. P. Dave, "Neuro-optical microfluidic platform to study injury and regeneration of single axons," *Lab Chip* **9**(17), 2576–2581 (2009).
9. A. Ghosh-Roy and A. D. Chisholm, "Caenorhabditis elegans: a new model organism for studies of axon regeneration," *Dev. Dyn.* **239**(5), 1460–1464 (2010).
10. G. Banker and K. Goslin, *Culturing Nerve Cells*, 2nd ed. G. Banker and K. Goslin, Eds., The MIT Press, Cambridge, MA (1998).
11. J. Rajagopalan, A. Tofangchi, and M. T. A. Saif, "Drosophila neurons actively regulate axonal tension *in vivo*," *Biophys. J.* **99**, 3208–3215 (2010).
12. D. Cojoc, F. Difato, E. Ferrari, R. B. Shahapure, J. Laishram, M. Righi, E. M. Di Fabrizio, and V. Torre, "Properties of the force exerted by filopodia and lamellipodia and the involvement of cytoskeletal components," *PLoS ONE* **2**(10), e1072 (2007).
13. F. Difato, E. Ferrari, R. Shahapure, V. Torre, and D. Cojoc, "Optical tweezers microscopy: pico-Newton forces in cell and molecular biology," Chap. 15 in *Nanoscopy and Multidimensional Optical Fluorescence Microscopy*, A. Diaspro, Ed., pp. 16-1-19, Taylor & Francis, Boca Raton, FL (2010).
14. G. Giannone, G. Jiang, D. H. Sutton, D. R. Critchley, and M. P. Sheetz, "Talin 1 is critical for force-dependent reinforcement of initial integrin-cytoskeleton bonds but not tyrosine kinase activation," *J. Cell Biol.* **163**(2), 409–419 (2003).
15. R. Shahapure, F. Difato, A. Laio, G. Bisson, E. Ercolini, L. Amin, E. Ferrari, and V. Torre, "Force generation in lamellipodia is a probabilistic process with fast growth and retraction events," *Biophys. J.* **98**(6), 979–988 (2010).
16. A. Rohrbach, "Switching and measuring a force of 25 femtoNewtons with an optical trap," *Opt. Express* **13**(24), 9695–9701 (2005).
17. H. Kress, E. H. Stelzer, D. Holzer, F. Buss, G. Griffiths, and A. Rohrbach, "Filopodia act as phagocytic tentacles and pull with discrete steps and a load-dependent velocity," *Proc Natl Acad Sci U.S.A.* **104**(28), 11633–11638 (2007).
18. J. Colombelli, E. G. Reynaud, and E. H. Stelzer, "Investigating relaxation processes in cells and developing organisms: from cell ablation to cytoskeleton nanosurgery," *Methods Cell Biol.* **82**, 267–291 (2007).
19. M. W. Berns and K. O. Greulich, *Methods in Cell Biology: Laser Manipulation of Cells and Tissues* **82**, Academic Press, San Diego (2007).
20. M. Allieux-Guerin, D. Icard-Arcizet, C. Durieux, S. Henon, F. Gallet, J. C. Mevel, M. J. Masse, M. Tramier, and M. Coppey-Moisan, "Spatio-temporal analysis of cell response to a rigidity gradient: a quantitative study by multiple optical tweezers," *Biophys. J.* **96**(1), 238–247 (2008).
21. D. E. Ingber, "Tensegrity and mechanotransduction," *J. Bodyw. Mov. Ther.* **12**(3), 198–200 (2008).

22. M. Stuess, N. Maghelli, L. C. Kapitein, S. Gomis-Ruth, M. Wilsch-Brauninger, C. C. Hoogenraad, I. M. Tolic-Norrelykke, and F. Bradke, "Axon extension occurs independently of centrosomal microtubule nucleation," *Science* **327**(5966), 704–707 (2010).
23. S. Siechen, S. Yang, A. Chiba, and T. Saif, "Mechanical tension contributes to clustering of neurotransmitter vesicles at presynaptic terminals," *Proc. Natl. Acad. Sci. U.S.A* **106**(31), 12611–12616 (2009).
24. D. C. Van Essen, "A tension-based theory of morphogenesis and compact wiring in the central nervous system," *Nature (London)* **385**(6614), 313–318 (1997).
25. B. C. Wheeler, J. M. Corey, G. J. Brewer, and D. W. Branch, "Microcontact printing for precise control of nerve cell growth in culture," *J. Biomech. Eng* **121**(1), 73–78 (1999).
26. C. O. Mejean, A. W. Schaefer, E. A. Millman, P. Forscher, and E. R. Dufresne, "Multiplexed force measurements on live cells with holographic optical tweezers," *Opt. Express* **17**(8), 6209–6217 (2009).
27. H. Kress, J. G. Park, C. O. Mejean, J. D. Forster, J. Park, S. S. Walse, Y. Zhang, D. Wu, O. D. Weiner, T. M. Fahmy, and E. R. Dufresne, "Cell stimulation with optically manipulated microsources," *Nat. Methods* **6**(12), 905–909 (2009).